

Sheared active fluids: Thickening, thinning, and vanishing viscosity

Luca Giomi,^{1,2} Tanniemola B. Liverpool,³ and M. Cristina Marchetti⁴

¹*School of Engineering and Applied Sciences, Harvard University, Cambridge, Massachusetts 02138, USA*

²*Martin A. Fisher School of Physics, Brandeis University, Waltham, Massachusetts 02454, USA*

³*Department of Mathematics, University of Bristol, Bristol BS8 1TW, United Kingdom*

⁴*Physics Department and Syracuse Biomaterials Institute, Syracuse University, Syracuse, New York 13244, USA*

(Received 9 February 2010; published 6 May 2010)

We analyze the behavior of a suspension of active polar particles under shear. In the absence of external forces, orientationally ordered active particles are known to exhibit a transition to a state of nonuniform polarization and spontaneous flow. Such a transition results from the interplay between elastic stresses, due to the liquid crystallinity of the suspension, and internal active stresses. In the presence of an external shear, we find an extremely rich variety of phenomena, including an effective reduction (increase) in the apparent viscosity depending on the nature of the active stresses and the flow-alignment property of the particles, as well as more exotic behaviors such as a nonmonotonic stress–strain-rate relation and yield stress for large activities.

DOI: [10.1103/PhysRevE.81.051908](https://doi.org/10.1103/PhysRevE.81.051908)

PACS number(s): 87.16.Ln, 42.70.Df, 87.18.Ed

I. INTRODUCTION

Colonies of swimming bacteria, *in vitro* mixtures of cytoskeletal filaments and motor proteins, and vibrated granular rods are examples of *active* systems composed of interacting units that consume energy and collectively generate motion and mechanical stresses. Due to their elongated shape, active particles can exhibit orientational order at high concentration and have been likened to “living liquid crystals” [1]. Their rich collective behavior includes nonequilibrium phase transition and pattern formation on mesoscopic scales [2–10]. It has been modeled by continuum equations built by modifying the hydrodynamics of liquid crystals to include nonequilibrium terms that account for the activity of the system [2–4] or derived from specific microscopic models [11,12].

A striking property of *confined* active liquid crystals is the instability of the uniform aligned homogeneous state and the onset of spontaneously flowing states, both stationary and oscillatory [13,14]. This occurs because local orientational order generates active stresses that are in turn balanced by flow, yielding a state that can support local inhomogeneities in the flow velocity and the local alignment, while maintaining a net zero force. Loosely speaking, a confined active liquid crystal “shears itself” even in the absence of externally applied forces. It is then not surprising that the rheology of such active liquid crystals in response to an external shear will be very rich.

Phenomenological work by Hatwalne *et al.* [15] first pointed out that activity lowers the linear bulk viscosity of tensile suspensions, such as most swimming bacteria, while it enhances the viscosity of contractile systems, and that this enhancement may become very large near the isotropic-nematic transition. A semimicroscopic model of contractile suspensions of motor-filaments mixtures confirmed these results and predicted an actual divergence of the viscosity of contractile suspensions at the transition [16]. Recent numerical studies of active nematic films by Cates *et al.* [17] confirmed that this result survives when the effect of boundaries is included. In addition, it was found that tensile nematic suspensions can enter a regime of vanishing apparent viscos-

ity in proximity of the isotropic-nematic phase transition. Such a “superfluid” window was interpreted by the authors of Ref. [17] as the appearance of bulk shear bands accommodating a range of macroscopic shear rates at zero stress. Finally, the predicted activity-induced thinning of bacterial suspensions has been demonstrated in recent experiments in *Bacillus subtilis* [18–20].

Active particles exert forces on the surrounding fluid, resulting in local tensile or contractile stresses proportional to the amount of orientational order, $\sigma_{ij}^\alpha \sim \alpha n_i n_j$, where α is proportional to the force exerted by the active particles on the fluid and \mathbf{n} a unit vector denoting the direction of broken orientational symmetry. The sign of α determines whether the flow generated by the active particles is tensile ($\alpha < 0$) or contractile ($\alpha > 0$). In the case of swimming organisms, the former situation describes “pushers,” i.e., most bacteria (e.g., *E. coli*), while the latter corresponds to “pullers” (e.g., *Chlamydomonas*) (see Fig. 1) [26]. An important distinction between uniaxial active particles concerns the possibility of forming phases with or without a nonzero macroscopic polarization. Apolar particles are fore-aft symmetric and can form nematic phases in which macroscopic quantities are invariant for $\mathbf{n} \rightarrow -\mathbf{n}$. Polar particles can also form phases characterized by a nonzero macroscopic polarization in the direction of a polar director \mathbf{p} in which they undergo collective motion with mean velocity $\mathbf{v} \sim \beta \mathbf{p}$, with β is the typical self-propulsion velocity. This directed motion occurring in

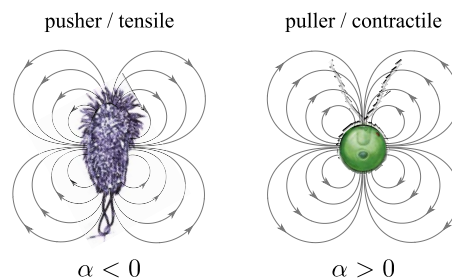


FIG. 1. (Color online) Schematic example of the flow field surrounding tensile (left) and contractile (right) swimming microorganisms.

polar suspensions contributes to a nonequilibrium local stress of the form $\sigma_{ij}^\beta \sim \beta(\partial_i p_j + \partial_j p_i)$.

Most theoretical works have focused on the rheology of active nematic ($\beta=0$), while the shear response of active polar suspensions is far less explored [18,20]. We find that for a fixed value of β , the behavior of active suspensions depends on the interplay between the local contractile or tensile stresses, embodied in the parameter α , and the flow-aligning behavior of liquid crystalline particles, described by the flow-alignment parameter λ . In passive liquid crystals, the magnitude of λ controls how the director field responds to a large shear flow away from boundaries. For $|\lambda| > 1$, the director tends to align to the flow direction at an angle θ_0 such that $\cos 2\theta_0 = 1/\lambda$, while for $|\lambda| < 1$, it forms rolls throughout the systems. These regimes are known as “flow aligning” and “flow tumbling,” respectively. The *hydrodynamic* coupling between local orientation and flow, embodied in the parameter λ , is a collective property of the system capturing the interaction between *many* active elements and the local flow velocity. The value of λ is mainly determined by the shape of the active particles. Rod-shaped particles typically have $\lambda > 0$, spherical particles have $\lambda = 0$, while the case $\lambda < 0$ describes disk-shaped molecules such as those found in discotic liquid crystals [21]. Understanding of the complex rheology of polar and nematic active suspensions requires exploring the full parameter space, including the important role of boundary conditions. One of the important results of this work is a remarkable exact duality that holds at small shear rates and shows that tensile ($\alpha < 0$) rod-shaped flow-aligning particles ($\lambda > 1$) are rheologically equivalent to contractile ($\alpha > 0$) discotic flow-tumbling particles ($-1 \leq \lambda < 0$). Using this result, we present below a unified description of the linear rheology of active suspensions of both polar and apolar particles. Some of the results are summarized in the “phase diagram” of Fig. 2. This figure shows that the rheological properties of an active film subject to an external shear are closely related to the onset of spontaneous flow in the absence of shear, highlighting the parallel role played in active system by mechanical driving forces, such as a macroscopic strain rate, and internal active driving forces proportional to α and β .

An unsheared active film exhibits a transition from the homogeneous aligned state to a “spontaneously flowing” state, characterized by spatially inhomogeneous velocity and director profiles [13]. The transition occurs at a critical activity α_{c1} in a film bounded by one no-slip substrate and a surface that can freely slide and at a larger value, $\alpha_{c2} > \alpha_{c1}$, in a film bounded by two no-slip planes. The lines separating regions of different shades in Fig. 2 are the boundaries $\alpha_{c1}(\beta, \lambda)$ [see Eq. (8) below] separating regions of spontaneous flow ($|\alpha| > \alpha_{c1}$) from regions where the homogeneous aligned state is stable ($|\alpha| < \alpha_{c1}$). Interestingly, when the film is subject to an external shear, we find that the flow properties change their *qualitative* behavior at exactly these same critical values of activity. For $\alpha_{c1} < |\alpha| < \alpha_{c2}$, the theoretical stress-strain rate curves obtained from our one-dimensional model are nonmonotonic (see Fig. 7) and the active suspension is strongly non-Newtonian. We suggest a number of different interpretations of the nonmonotonic part of the stress-strain rate curve shown in Fig. 8. These include mac-

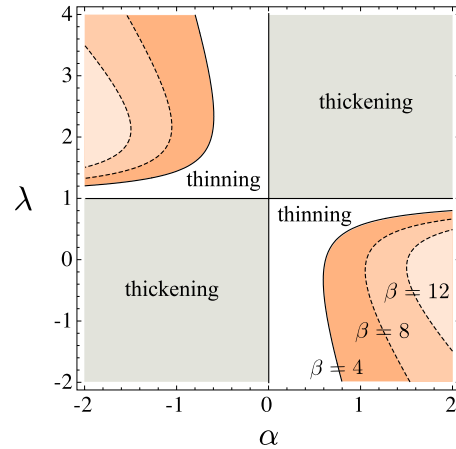


FIG. 2. (Color online) Regions of parameters where spontaneous flow occurs in an unsheared active film on a substrate. The regions of spontaneous flow are bounded by the critical activity $\alpha_{c1}(\beta)$ given in Eq. (8) (solid and dashed lines) and are shaded orange, with lighter shades corresponding to increasing values of β . The same critical activity also separates the regions $|\alpha| < \alpha_{c1}$ where the theoretical stress-strain curves are monotonic and the active suspension is either thinned or thickened by activity at small shear rates, as indicated, from the regions $|\alpha| > \alpha_{c1}$ where the theoretical stress-strain curves are nonmonotonic, with possible “superfluid” or hysteretic behavior.

roscopic “superfluidlike” behavior [17] with zero effective viscosity, yield-stress behavior, or hysteresis. Finally, for $|\alpha| > \alpha_{c2}$, the theoretical stress-strain curve has a discontinuous jump at zero strain rate, corresponding to a finite “spontaneous stress” in the absence of applied shear [16].

II. MODEL

Our model of active suspension consists of a two-dimensional film of rodlike particles of length ℓ confined to a channel of infinite length along the x axis and finite thickness L along the y axis (see Fig. 3). Because of the chosen geometry, the system is invariant for translations along the x axis. The total density of the suspension, $\rho = Mc + \rho_{\text{solvent}}$, with c the concentration of active particles and M their mass, is assumed to be constant, thus $\nabla \cdot \mathbf{v} = 0$, with \mathbf{v} the flow ve-

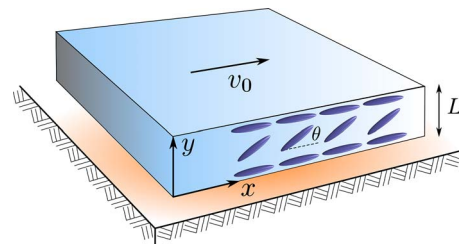


FIG. 3. (Color online) Schematic representation of a quasi-one-dimensional film of thickness L . In our model, the film is sitting on a nonslipping surface and is sheared from the top at constant velocity v_0 . The polar rods form an angle θ with respect to the infinite direction x of the film. Because of the quasi-one-dimensional geometry, the system is invariant for translations along the x axis.

locity. We assume that the film is sheared at a constant (macroscopic) rate $\dot{\gamma}$ by keeping the lower plate at $y=0$ fixed, while the upper plate at $y=L$ is moved at constant velocity v_0 . The macroscopic shear rate is defined then as $\dot{\gamma}=v_0/L = \int_0^L (dy/L)u$, where the rate-of-strain tensor $u_{ij}=(\partial_i v_j + \partial_j v_i)/2$ has only nonzero components $u_{xy}=u_{yx}=\partial_y v_x/2 \equiv u/2$. Theoretical stress-strain curves are obtained by fixing the macroscopic strain rate $\dot{\gamma}$ and calculating the resulting stress σ .

We consider a polarized active suspension and focus only on spatial variations in the direction of the polarization \mathbf{P} . The hydrodynamic equations for an active polar suspension have been formulated by incorporating the active contributions (proportional to the rate of energy consumed by the active units) into the hydrodynamic equations of a passive polar liquid crystalline film. Some of the active contributions, discussed above, are not allowed by the conditions which define liquid crystal systems at equilibrium and hence are *intrinsic* to active systems. Other terms have the same form as those of passive polar liquid crystals and can simply be included by modifying the prefactors of the terms obtained from a passive system. As such, the modified “passive” contributions to the equations of motion can be described starting from the nonequilibrium analog of the Frank free energy of a suspension of polar particles in a solvent

$$F = \int_{\mathbf{r}} \left\{ \frac{C}{2} \left(\frac{\delta c}{c_0} \right)^2 + \frac{a_2}{2} |\mathbf{P}|^2 + \frac{a_4}{4} |\mathbf{P}|^4 + \frac{K_1}{2} (\nabla \cdot \mathbf{P})^2 + \frac{K_3}{2} (\nabla \times \mathbf{P})^2 + B_1 \frac{\delta c}{c_0} \nabla \cdot \mathbf{P} + B_2 |\mathbf{P}|^2 \nabla \cdot \mathbf{P} + \frac{B_3}{c_0} |\mathbf{P}|^2 \mathbf{P} \cdot \nabla c \right\},$$

with C the compressional modulus and K_1 and K_3 the splay and bend elastic constants. The parameters a_i, B_i, K_i, C are understood to have both passive and active contributions. In the following, we will take $K_1=K_3=K$. The last three terms in the expression of the free-energy couple concentration and splay and are also present in equilibrium polar suspensions.

The dynamics of the concentration and the polarization are described by

$$\partial_t c = -\nabla [c(\mathbf{v} + c\beta_1 \mathbf{P}) + \Gamma' \mathbf{h} + \Gamma' \mathbf{f}], \quad (1a)$$

$$[\partial_t + (\mathbf{v} + c\beta_2 \mathbf{P}) \cdot \nabla] P_i + \omega_{ij} P_j = \lambda u_{ij} P_j + \Gamma h_i + \Gamma' f_i, \quad (1b)$$

with $\omega_{ij}=(\partial_i v_j - \partial_j v_i)/2$ the vorticity tensor, $\mathbf{h}=-\delta F/\delta \mathbf{P}$ the molecular field, and $\mathbf{f}=-\nabla(\delta F/\delta c)$. The flow velocity satisfies the Navier-Stokes equation [27]

$$\rho(\partial_t + \mathbf{v} \cdot \nabla) v_i = \partial_j \sigma_{ij}, \quad (2)$$

with $\nabla \cdot \mathbf{v}=0$ to guarantee incompressibility, and stress tensor given by dissipative, reversible, and active contributions, $\sigma_{ij}=2\eta u_{ij} + \sigma_{ij}^r + \sigma_{ij}^\alpha + \sigma_{ij}^\beta$, with

$$\sigma_{ij}^\alpha = \frac{\alpha c^2}{\Gamma} (P_i P_j + \delta_{ij}), \quad (3a)$$

$$\sigma_{ij}^\beta = \frac{\beta_3 c^2}{\Gamma} [\partial_i P_j + \partial_j P_i + \delta_{ij} \nabla \cdot \mathbf{P}], \quad (3b)$$

$$\sigma_{ij}^r = -\Pi \delta_{ij} - \frac{\lambda}{2} (P_i h_j + P_j h_i) + \frac{1}{2} (P_i h_j - P_j h_i), \quad (3c)$$

where Π is the pressure, η the shear viscosity, and we have assumed an isotropic viscosity tensor. We now consider a solution deep in the polarized state and neglect fluctuations in the magnitude of the polarization, i.e., assume $|\mathbf{P}| = \sqrt{-a_2/a_4}$. For simplicity, we also redefine units so that $|\mathbf{P}| = 1$. The condition $\mathbf{P}=\text{const}$ determines the longitudinal part $h_{\parallel}=\mathbf{p} \cdot \mathbf{h}$ of the molecular field that can then be eliminated from the hydrodynamic equations. The details associated with imposing the constancy of the magnitude of the polarization and deriving the hydrodynamic equations solely in terms of the polar director $\mathbf{p}=\mathbf{P}/|\mathbf{P}|$ are given in the Appendix. With this choice, the hydrodynamic equations for \mathbf{p} and c can be written in the form

$$\partial_t c + \nabla \cdot c(\mathbf{v} + \beta_1 c \mathbf{p}) = \partial_i [D_{ij} \partial_j c + \lambda \gamma' u_{ki} p_k p_l p_i], \quad (4a)$$

$$[\partial_t + (\mathbf{v} + \beta_2 c \mathbf{p}) \cdot \nabla] p_i + \omega_{ij} p_j = \delta_{ij}^T \left[\lambda u_{jk} p_k + \frac{w}{c_0} \partial_t c - \frac{\gamma' w}{c_0} \partial_j \nabla \cdot \mathbf{p} + \kappa \nabla^2 p_j \right], \quad (4b)$$

with $\gamma'=\Gamma'/\Gamma$, $\kappa=\Gamma K$, $w=\Gamma(B_1-B_3)$, and $\delta_{ij}^T=\delta_{ij}-p_i p_j$ the transverse projection operator. D_{ij} is an effective diffusion tensor given by

$$D_{ij} = D_1 \delta_{ij} + D_2 p_i p_j, \quad (5)$$

where $D_1=D-\gamma'w/c_0$ and $D_2=\gamma'w/c_0-D\xi$. Finally, the reversible part of the stress tensor σ_{ij}^r becomes

$$\begin{aligned} \sigma_{ij}^r = & -\delta_{ij} \Pi + \lambda p_i p_j p_k \left[\frac{w}{c_0 \Gamma} \partial_k c + K \nabla^2 p_k \right] \\ & - \frac{\lambda}{2} \left[\frac{w}{c_0 \Gamma} (p_i \partial_j c + p_j \partial_i c) + K (p_i \nabla^2 p_j + p_j \nabla^2 p_i) \right] \\ & + \frac{1}{2} \left[\frac{w}{c_0 \Gamma} (p_i \partial_j c - p_j \partial_i c) + K (p_i \nabla^2 p_j - p_j \nabla^2 p_i) \right] \\ & - \lambda \Gamma' \xi p_i p_j (D p_k \partial_k c + w p_k \partial_k p_l) + \frac{\lambda^2}{\Gamma} p_i p_j u_{kl} p_k p_l. \end{aligned}$$

The equations for an active suspension have been written down phenomenologically and also derived from various semimicroscopic models. The structure of the equations is generic and applies to a broad class of “living liquid crystals.” The parameters in the equations are of course system and model specific. In motor-filament mixtures, activity arises from clusters of motor proteins crosslinking pairs of filaments. The active couplings are therefore of order c^2 in this case [11,12]. In suspensions of swimming microorganisms, activity can be described in terms of the active force f that each swimmer exerts on the surrounding fluid. In this case, the active couplings arise even at the single-swimmer level and are of order c [22]. Estimates for the active parameters obtained from semimicroscopic models are summarized

TABLE I. Estimates of active parameters for two types of active suspensions: (i) mixtures of cytoskeletal filaments and cross-linking motor proteins [11,12,23], with \tilde{m} a dimensionless density of crosslinking motor clusters, u_0 the speed at which motor proteins walk on filaments, in turn proportional to the rate of adenosine triphosphate (ATP) consumption, and $|u_1| \sim u_0 \ell_m$, with ℓ_m the size of a motor cluster; and (ii) swimming microorganisms [22], where $v_{sp} \sim (f/\zeta)\epsilon$ is the self-propulsion speed of an individual organisms, with f the force that swimmers exert on the fluid, $\epsilon < 1$ a dimensionless number determined by the shape of the swimmer, and $\zeta \sim 1/\Gamma$ is the longitudinal friction coefficient of a rodlike swimmer of length ℓ . For both systems, the precise values of parameters obtained from each microscopic model differ from the above by numerical constants of order unity.

	Filaments-motors (\sim)	Swimmers (\sim)
β_1	$\tilde{m}u_0\ell^2$	v_{sp}/c
β_2	$-\tilde{m}u_0\ell^2$	v_{sp}/c
w	$\tilde{m}u_0\ell^2$	$-v_{sp}/c$
α	$\tilde{m}u_1\ell^2$	$f\ell^3/(\zeta c)$
β_3	$\tilde{m}u_0\ell^2$	v_{sp}/c

in Table I. The equations for an active nematic can be obtained from those of a polar systems by setting $\beta_i = w = 0$. In the following, we assume $\beta_1 = \beta_3 = -\beta_2 = \beta$, as appropriate for motor filament systems.

It is convenient to work with dimensionless quantities. Spatial variables are normalized with the length ℓ of the rods. Thus, $y \rightarrow y/\ell$. Temporal variables are normalized with the time scale of splay and bending fluctuations, thus $t \rightarrow t/\tau$, where $\tau = \ell^2/\kappa$. A mass scale is set by τ/Γ . All the other quantities are normalized accordingly. In these units, the hydrodynamic equations for the rods concentration $\phi = c/c_0$, with c_0 the mean density, and the director-polarization angle θ , with $\mathbf{p} = (\cos \theta, \sin \theta)$, for the geometry of interest are

$$\rho(\partial_t + v_y \partial_y) v_x = \partial_y \sigma_{xy}, \quad (6a)$$

$$\partial_t \phi = \partial_y \{ \beta \phi^2 \sin \theta + \mathcal{D}(\theta) \partial_y \phi + \lambda u \sin \theta \sin 2\theta \}, \quad (6b)$$

$$\begin{aligned} \partial_t \theta = & -\beta \phi \sin \theta \partial_y \theta + w \cos \theta \partial_y \phi + \mathcal{K}(\theta) \partial_y^2 \theta \\ & + w \cos \theta \sin \theta (\partial_y \theta)^2 - u(1 - \lambda \cos 2\theta), \end{aligned} \quad (6c)$$

where $\mathcal{D}(\theta) = D(1 - \xi \sin^2 \theta) - w \cos^2 \theta$ is a diffusion coefficient, $\mathcal{K}(\theta) = 1 - w \cos^2 \theta$ describes the energy cost of bend and splay deformations, and λ is the flow-alignment parameter. In a steady state, the stress tensor $\sigma_{xy} \equiv \sigma$ is constant across the film and it is given by

$$\begin{aligned} \sigma = & u[\eta + \lambda^2 \sin^2 2\theta] + \lambda w \sin^2 \theta \sin 2\theta (\partial_y \theta)^2 \\ & + [w - \lambda w_0 - \lambda(w - w_0) \cos 2\theta] \cos \theta \partial_y \phi + \alpha \phi^2 \sin 2\theta \\ & - 2\beta \phi^2 \sin \theta \partial_y \theta, \end{aligned} \quad (7)$$

with η the bare viscosity and w_0 a constant proportional to the ratio between the translational and orientational diffusion coefficients (i.e., $w_0 \sim D/K$). Our goal is to study the relation

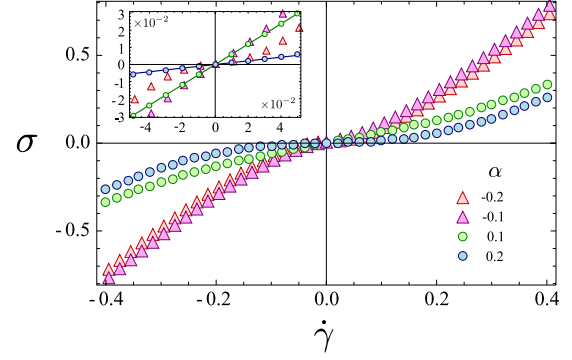


FIG. 4. (Color online) Stress (σ) vs strain ($\dot{\gamma}$) for an active nematic ($\beta=w=0$) suspension for various α . Flow-tumbling systems with $\lambda=0.1$ are marked by circles and flow-aligning systems with $\lambda=1.9$ by triangles. Other parameters are set $L/\ell=5$, $\eta=1$, $\phi_0=1$, $D=1$, and $\xi=0.3$. Inset shows the comparison to the analytical result given in Eq. (9).

between the induced shear stress σ and the applied shear rate $\dot{\gamma}$ as a function of the two fundamental active parameters α and β representing the magnitude of the internal contractile-tensile stress and the velocity scale of directed motion. In order to construct a σ vs $\dot{\gamma}$ map, we integrate Eqs. (6) numerically with boundary conditions $v_x(0)=0$ and $v_x(L)=v_0$, $\theta(0)=\theta(L)=0$ and $j_y(0)=j_y(L)=0$, which implies $\phi'(0)=\phi'(L)=0$. As initial conditions, we choose $\theta(y,0)=0$ and $\phi(y,0)=1$.

In the absence of applied shear, active polar and nematic films exhibit a transition from a quiescent ($v_x=0$) aligned ($\theta=0$) state to a state of spontaneous flow, with both inhomogeneous alignment and velocity profiles. The critical value of activity where the instability occurs depends on boundary conditions. For a film bounded by a no-slip substrate and a surface that can freely slide, it is given by [14]

$$\alpha_{c1}(\beta, \lambda) = \left(\frac{\pi}{L} \right)^2 \frac{\eta(1-w)}{2\phi_0^2(1-\lambda)} + \frac{\beta w[\eta + (1-\lambda)^2]}{2(1-\lambda)(D-w)} \quad (8)$$

and the spontaneously flowing state has $\sigma=0$. For a film bounded by two no-slip surfaces, the critical value is $\alpha_{c2} = 4\alpha_{c1}$ and the spontaneously flowing state is characterized by a finite value of σ . The regions of spontaneous flow in the (λ, α) plane are displayed in shades of orange in Fig. 2. In these regions, the film exhibits strongly nonlinear rheology, with nonmonotonic stress-strain curves, as described below.

III. LINEAR RHEOLOGY OF WEAKLY ACTIVE SYSTEMS

For $|\alpha| < \alpha_{c1}$, corresponding to the gray regions of Fig. 2, the stress-strain curves are monotonic and remain linear over a broad range of $\dot{\gamma}$, as shown in Fig. 4. Non-Newtonian behavior sets in at smaller values of $\dot{\gamma}$ with increasing α . As the value of α is increased, the slope of the linear portion of the stress-strain curves for $\alpha < \alpha_{c1}$ decreases with increasing α , indicating that contractile active stresses lower the effective viscosity of the system. The effective linear viscosity can be calculated analytically by solving Eqs. (6c) and (6b) pertur-

batively in σ by expanding the fields θ and ϕ as $\theta = \theta_0 + \sigma\theta_1 + \sigma^2\theta_2 \dots$ and $\phi = \phi_0 + \sigma\phi_1 + \sigma^2\phi_2 \dots$. The quantities θ_0 and ϕ_0 represent here the stationary solution of the hydrodynamic equations in absence of shear flow. If the suspension is in an aligned state at $t=0$, when the shear is switched on, then $\theta_0=0$ and $\phi_0=\text{const}$. We note, however, that this perturbation analysis breaks down in the region $\alpha > \alpha_{c1}$ of spontaneous flow, as in that case both θ, ϕ are spatially varying even at $\sigma=0$. It is straightforward to solve Eqs. (6c) and (6b) to first order in σ . We then obtain the linear apparent viscosity defined as $\eta_{\text{app}} = \lim_{\dot{\gamma} \rightarrow 0} \sigma / \dot{\gamma}$ and given by

$$\eta_{\text{app}} = \frac{\eta(1 + \zeta)}{\zeta + \text{tanc}\left(\frac{kL}{2}\right)}, \quad (9)$$

where $\text{tanc}(x) = \tan(x)/x$ and

$$\zeta = \frac{\eta w \beta}{(1 - \lambda)[\beta w(1 - \lambda) - 2\alpha(D - w)]}, \quad (10a)$$

$$k^2 = \frac{2\alpha\phi_0^2(1 - \lambda)}{\eta(1 - w)} - \frac{\beta w \phi_0^2}{(1 - w)(D - w)} \left[1 + \frac{(1 - \lambda)^2}{\eta} \right]. \quad (10b)$$

For passive system $\alpha = \beta = w = 0$ and $\eta_{\text{app}} = \eta$, as expected. For active nematic, $\beta = w = 0$ and the apparent viscosity is simply

$$\eta_{\text{app}} = \frac{\eta}{\text{tanc}\left(\frac{kL}{2}\right)}, \quad (11)$$

with $k = \sqrt{2\alpha\phi_0^2(1 - \lambda)/\eta}$. If $\alpha(1 - \lambda) < 0$, k is imaginary and the tan function at the denominator of η_{app} is replaced by its hyperbolic counterpart. Since $\tanh(x)$ increases more slowly than x , the resulting apparent viscosity will increase. If $\alpha(1 - \lambda) > 0$, k is real and since the $\tan(x)$ function grows more rapidly than x , we expect then a rapid decrease in the apparent viscosity as $|\alpha|$ is increased. This shows that the linear rheology of pullers-tractile systems with $\lambda < 1$ are the same as those of pushers-tensile systems with $\lambda > 1$. From Eq. (9) it is indeed simple to prove that the apparent viscosity η_{app} is invariant under the transformation

$$\eta_{\text{app}}(\alpha, \beta, \lambda) = \eta_{\text{app}}(-\alpha, \beta, 2 - \lambda). \quad (12)$$

Thus flow-aligning pullers with $\lambda = 1 + \epsilon$ (for $0 \leq \epsilon < 1$) will exhibit the same apparent viscosity of flow-tumbling pushers with $\lambda = 1 - \epsilon$: $\eta_{\text{app}}(-|\alpha|, \beta, 1 + \epsilon) = \eta_{\text{app}}(|\alpha|, \beta, 1 - \epsilon)$. This duality is displayed in the top frame of Fig. 5 that shows the linear apparent viscosity of active nematic suspensions as a function of $|\alpha|$ for several values of λ . The solid curves (red online) show that both contractile-flow tumbling suspensions and tensile-flow-aligning ones are thinned by activity. The dashed curves (blue online) refer to either contractile-flow aligning suspensions or tensile-flow-tumbling ones and show that these systems are thickened by activity. Bacteria such as *E. coli* are pushers ($\alpha < 0$) and generally elongated in shape, corresponding to $\lambda > 1$. Our results therefore confirm the activity-induced thinning of bacterial suspensions first

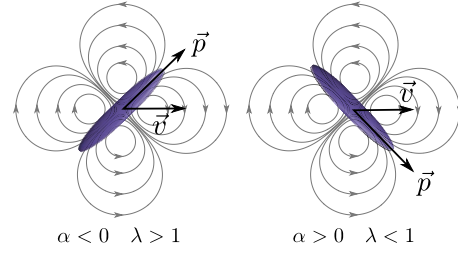


FIG. 5. (Color online) Schematic example of the flow field surrounding tensile-flow-aligning (right) and contractile-flow-tumbling active particles. For the choice of the parameters α and λ given in Eq. (12), the two flows are identical, leading to an equal apparent viscosity.

predicted by Hatwalne *et al.* [15] and recently observed in [19]. In contrast, the algae *Chlamydomonas* that propel themselves from the front (and are therefore pullers, with $\alpha > 0$). Whether they are thickened or thinned by activity depends intimately on their shape, i.e., on whether they can be described as objects with $\lambda > 1$ or $\lambda < 1$. Similarly, motor-filament mixtures are generally contractile ($\alpha > 0$) and are expected to be thickened or thinned by activity depending on the effective value of λ .

This duality has a simple interpretation. Active contractile (tensile) particles produce an ingoing (outgoing) flow in the surrounding fluid, but while flow-aligning particles orient at a positive angle with respect to the flow direction, flow-tumbling particles orient at a negative angle under a small applied shear (see Fig. 6). As a result, the average flow fields produced in the surrounding fluid are identical in the two cases and produce the same resistance to the imposed shear flow. This equivalence holds only for small applied shear stresses. For large shear rates, the configuration of the director field of a flow-tumbling suspension is dramatically different from that of flow-aligning one and the similarity between the two flow fields no longer holds.

IV. NONLINEAR RHEOLOGY OF STRONGLY ACTIVE SYSTEMS

The linear apparent viscosity given by Eq. (11) vanishes at $\alpha = \alpha_{c1}$, suggesting the onset of a superfluidlike behavior above this critical value of activity [17]. For $\alpha > \alpha_{c1}$, the linearized approximation breaks down and the stress versus (average) strain rate curve obtained by numerical solution of the equations is nonlinear and nonmonotonic, as shown in Fig. 7. We emphasize that the flow profiles are always inhomogeneous with varying velocity gradients and director orientation. For $\alpha_{c1} < \alpha < \alpha_{c2}$, the theoretical stress versus macroscopic (average) strain rate curve goes through the origin and exhibits a region of negative $d\sigma/d\dot{\gamma}$ that would in principle be mechanically unstable. What would be measured in an experiment would, however, depend critically on details of the experimental procedure and the particular apparatus. To study the steady-state rheology, there are in general two natural classes of experiments: either (i) one tunes the stress σ and measures the resulting strain rate $\dot{\gamma}$ or (ii) one does a sweep through the values of strain rate $\dot{\gamma}$ and measures the

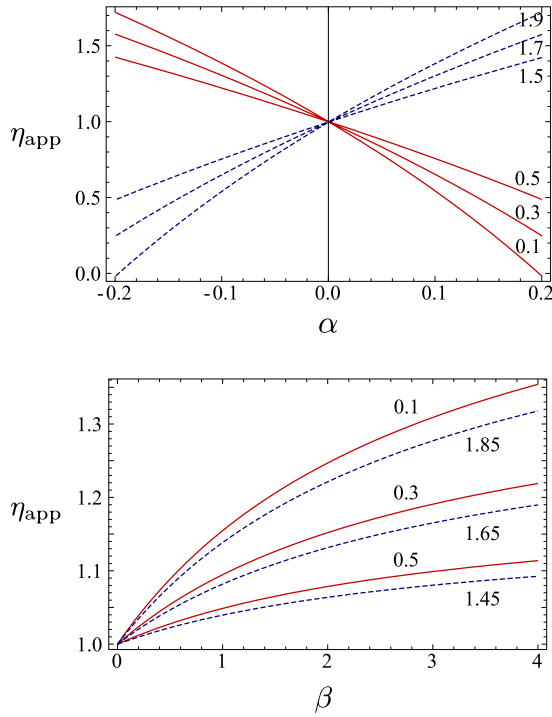


FIG. 6. (Color online) Apparent viscosity η_{app} for active nematic (top) and polar (bottom) suspensions from Eq. (9). Solid (red) lines represent flow-tumbling systems ($\lambda < 1$) while dashed (blue) lines represent flow-aligning systems ($\lambda > 1$). The corresponding values of λ are indicated next to the lines. In the bottom plot, α was set to zero. Top frame emphasizes the duality discussed in the text.

stress σ . If the stress-strain rate curve is monotonic, the two procedures are expected to yield the same result. However, this is no longer the case as soon as the response exhibits nonmonotonicity.

An important question, then, is what is the shape of the stress-strain rate curve that would be obtained experimentally for $\alpha > \alpha_{c1}$ in an experiment where one tunes the macroscopic strain rate $\dot{\gamma}$. Several scenarios are possible, as shown in Fig. 8 for a nonmonotonic curve with maximum or minimum at $\pm\sigma_m$.

(i) One scenario, suggested recently [17] based on numerical studies in the proximity of the isotropic-nematic phase transition and for small value of the active stress α , is the appearance of bulk shear bands accommodating a range of macroscopic shear rates at zero stress. This would correspond to the bulk stress-strain curve displayed in the top right frame of Fig. 8 and characterized as “superfluid” behavior. In the simplest picture, the sheared suspension would separate in bands of constant and opposite strain rates, each with zero stress. For the systems studied here (deep in the ordered phase, either nematic or polar), we find that the equations of motion provide no mechanism for selecting a particular value of the stress plateau and are unable to find a stable stress plateau at any value of $|\sigma| < \sigma_m$ (including $\sigma = 0$, see Fig. 8). Furthermore, we always find flow profiles with continuously varying gradients of fluid velocity for all values of macroscopic strain rate $\dot{\gamma}$, implying that the picture of two bands of constant strain rate would be at best an idealization.

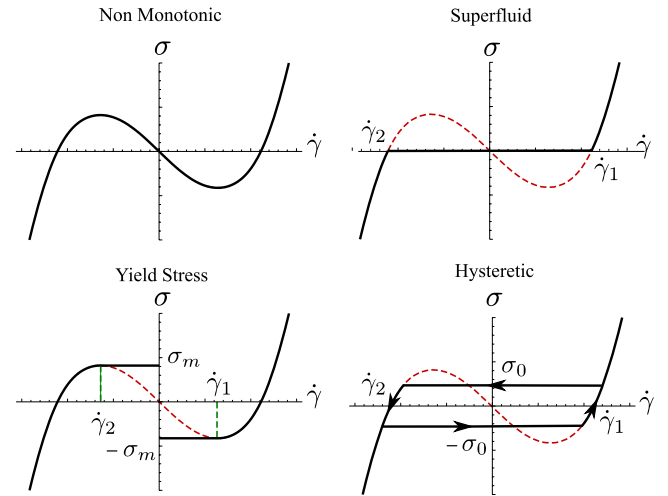


FIG. 7. (Color online) Top left frame displays a typical theoretical stress-strain curve of a nematic active suspension in the region $\alpha_{c1} < |\alpha| < \alpha_{c2}$. The theoretical curve is obtained by tuning $\dot{\gamma}$ and calculating the resulting σ and exhibits a region of $d\sigma/d\dot{\gamma} < 0$. The other three frames show three possible experimental stress-strain curves obtained by tuning σ and measuring $\dot{\gamma}$ that could be consistent with the theoretical curve. Top right frame displays the superfluid scenario suggested in [17], with bulk shear bands accommodating different macroscopic shear rates and zero net stress, so that the apparent viscosity of the system is simply zero. Bottom left frame shows a yield-stress-like behavior with a yield stress $\sigma_y = \sigma_m$. The last scenario is described in the bottom right frame and corresponds to a hysteretic stress-strain curve where the suspension can accommodate a range of macroscopic strain rates maintaining a constant total stress $\pm\sigma_0$.

(ii) An alternative scenario that is observed in other driven systems, such as charge-density waves in anisotropic metals [24] and collections of motor proteins [25], is shown in the bottom right frame of Fig. 8. In this case, the system is expected to exhibit hysteresis, with regions that accommodate coexistence of a range of macroscopic strain rates, corresponding to the constant value $\pm\sigma_0$ of applied stress. In general, σ_0 may coincide with σ_m or may be lower, with the system exhibiting “early switching.” The width of the hori-

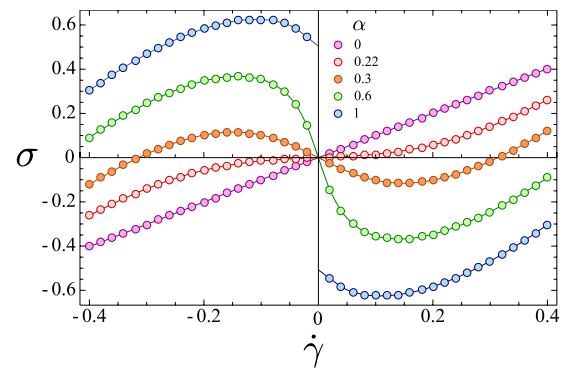


FIG. 8. (Color online) Stress-strain curves of a nematic suspension ($\beta = w = 0$) obtained by numerical solution of the active hydrodynamic equations for several values of α . $\alpha_{c1} = 0.219$ and $\alpha_{c2} = 0.877$ for the parameters chosen in the numerical solution.

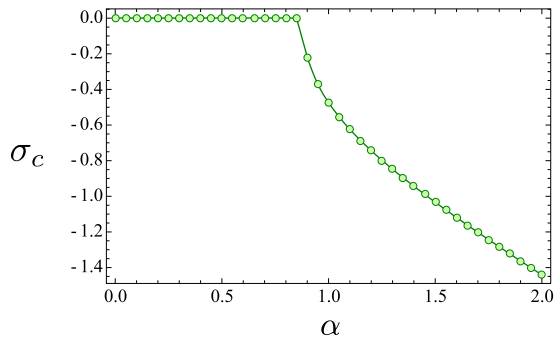


FIG. 9. (Color online) Yield stress σ_c as a function of α for a nematic suspension ($\beta=w=0$) obtained by numerical solution of the active hydrodynamic equations.

zontal hysteretic region of the stress-strain curve decreases with increasing α . In this picture, the particular steady-state behavior observed will depend on the initial conditions and particular flow history of each sample.

(iii) Another possibility is that the system shows a yield-stress-like behavior with a yield stress $\pm\sigma_y$, whose sign is determined by the direction of the flow. The value of the yield stress could also be anywhere in the “unstable” range of stress: $\sigma_y \leq \sigma_m$.

(iv) Finally, there is one more possibility: that the theoretical curve would indeed be reproduced by an experiment which scanned through different values of the macroscopic strain rate. The theoretical curve has been calculated by fixing $\dot{\gamma}$ and calculating the corresponding value of σ under the assumption that there are variations in the director and flow field *only* in the gradient direction (i.e., perpendicular to the plates). If this *assumption* is valid, every point on this curve does therefore represent a stable state corresponding to this procedure.

For $\alpha > \alpha_{c2}$, the stress-strain curve intercepts the $\dot{\gamma}=0$ axis at a finite value $\sigma_c = \sigma(\dot{\gamma}=0)$ of the strain rate. The active suspension has a nonzero spontaneous stress even in the absence of applied forces, as indeed observed in the spontaneous flow regime of an active suspension confined between two stationary no-slip planes. In other words, a finite force must be applied to the active suspension to keep it from sliding even at zero mean strain rate. This spontaneous stress σ_c is shown as a function of α in Fig. 9. The sign of the stress determines the direction of spontaneous flow.

We now speculate on the possible behavior of the system for each of the scenarios sketched above as α goes through α_{c2} . The behavior is shown schematically in Fig. 10. (i) In the superfluid scenario, the response of the suspension to an applied macroscopic strain rate will show yield-stress behavior. The system would smoothly go from the zero-stress plateau to a yield stress which increases from zero at α_{c2} . (ii) In the hysteretic scenario, the minimum height of the hysteretic loop becomes $2\sigma_c$, i.e., $\sigma_c \leq \sigma_0 \leq \sigma_m$. (iii) In the yield-stress scenario, the system already shows yield-stress behavior which continues for $\alpha > \alpha_{c2}$. (iv) In the nonmonotonic scenario, the nonmonotonic stress-strain rate curve shows a jump at $\dot{\gamma}$ whose magnitude increases from zero at α_{c2} .

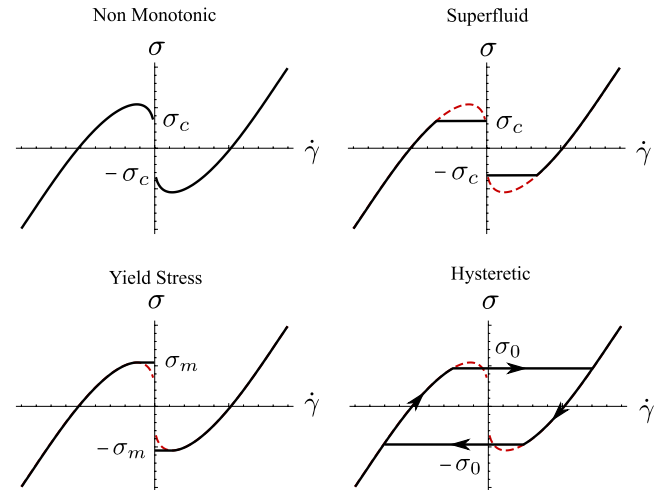


FIG. 10. (Color online) Possible scenarios for the transition to the yield-stress regime at $\alpha > \alpha_{c2}$. The nonmonotonic curve obtained numerically is shown in the top left frame. In the superfluid scenario (top-right), the plateau at $\sigma=0$ divides into two disconnected branches terminating at $\sigma = \pm\sigma_c$. In this case, the yield stress is expected to grow monotonically from zero. In the yield-stress scenario (bottom-left), there is already a nonzero stress at $\dot{\gamma}=0$ and thus the yield stress simply continues increasing with no qualitative change in the behavior at α_{c2} . In the hysteretic scenario (bottom-right), the loop intersects the positive σ axis at $\pm\sigma_0$, with $\sigma_c \leq \sigma_0 \leq \sigma_m$.

V. DISCUSSION AND CONCLUSIONS

We have studied the rheological behavior of a thin film of polar and apolar active materials. For weakly active systems, in the regime of the linear rheology, we have confirmed analytically the prediction of Hatwalne *et al.* [15] that activity can lower the linear bulk viscosity of tensile suspensions of swimmers as well as enhance the viscosity of contractile systems. We have shown that this result applies also for finite systems, in the presence of boundaries.

An important result of our work is the role of the *shape* of the active particles in controlling the rheological behavior. We find a remarkable exact duality that holds in the regime where the stress-strain rate relation is linear and shows that tensile ($\alpha < 0$) rod-shaped flow-aligning particles ($\lambda > 1$) are rheologically equivalent to contractile ($\alpha > 0$) discotic flow-tumbling particles ($-1 \leq \lambda < 0$). This means that activity lowers the linear viscosity of both tensile, rod-shaped particle and contractile, disk-shaped particle suspensions, while it increases the linear viscosity of contractile, rod-shaped particle and tensile, discotic particle suspensions.

For strongly active systems, we find that the rheological response is intrinsically nonlinear. The regime of linear rheology at small strain rates vanishes beyond a critical value of activity. In this strongly active regime, we explore a number of possible scenarios for the nonlinear rheology which include a superfluid phase with vanishing viscosity, hysteresis, yield-stress behavior, and nonmonotonic behavior. Our one-dimensional analysis does not, however, allow us to determine which of these scenarios is more likely. It is of course possible that allowing for variations of the director and flow

field in higher dimensions or allowing for variations in the magnitude of the order parameter would yield a criterion for selecting one of the proposed scenarios.

ACKNOWLEDGMENTS

L.G. was supported by NSF through the Harvard MRSEC and the Brandeis MRSEC and by the Harvard Kavli Institute for Nanobio Science and Technology. M.C.M. was supported by NSF Grants No. DMR-075105 and No. DMR-0806511. T.B.L. acknowledges the support of EPSRC-GB under Grant No. EP/G026440/1. We thank Suzanne Fielding and James Adams for illuminating discussions.

APPENDIX: DERIVATION OF EQS. (3)

In this section, we show some details of the derivation of the modified “passive” terms in the equation for the director field \mathbf{p} in the polarized state, when fluctuations in the magnitude of the order parameters are neglected. The equation for the full vector order parameter \mathbf{P} has the form

$$[\partial_t + \mathbf{v} \cdot \nabla]P_i = \lambda u_{ij}P_j + \Gamma h_i + \Gamma' f_i. \quad (\text{A1})$$

Equation (A1) can be separated in two equations for the magnitude $P=|\mathbf{P}|$ of the polarization and its direction $\mathbf{p}=\mathbf{P}/P$ using

$$\partial_t P = p_i \partial_t P_i, \quad (\text{A2})$$

$$\partial_t p_i = \frac{1}{P} \delta_{ij}^T \partial_t P_j, \quad (\text{A3})$$

where $\delta_{ij}^T = \delta_{ij} - p_i p_j$ is a transverse projection operator, with the result

$$\partial_t P = P(\lambda u_{ij} p_i p_j) + \Gamma' f_{\parallel} + \Gamma h_{\parallel},$$

$$[\partial_t + \mathbf{v} \cdot \nabla]p_i + \omega_{ij} p_j = \lambda \delta_{ij}^T u_{jk} p_k + \frac{1}{P} (\Gamma' f_i^{\perp} + \Gamma h_i^{\perp}),$$

where we have defined

$$h_{\parallel} = \mathbf{p} \cdot \mathbf{h}, \quad h_i^{\perp} = \delta_{ij}^T h_j, \quad f_{\parallel} = \mathbf{p} \cdot \mathbf{f}, \quad f_i^{\perp} = \delta_{ij}^T f_j.$$

In the ordered state, fluctuations in the magnitude P of the polarization are overdamped and will be neglected. We can

assume, on the other hand, to be deeply in the polarized state and that $P=\sqrt{-a_2/a_4}$ is constant. For simplicity, we redefine the units so that $P=1$. The condition $P=\text{const}$ determines the longitudinal part h_{\parallel} of the molecular field. This requires

$$h_{\parallel} = -\frac{1}{\Gamma} [\Gamma' f_{\parallel} + \lambda u_{ij} p_i p_j].$$

The above expression can be now used to eliminate h_{\parallel} from the density $\mathbf{j}=\Gamma' \mathbf{h} + \Gamma' \mathbf{f}$ appearing at the right-hand side of Eq. (1a). Expressing $h_i = p_i h_{\parallel} + h_i^{\perp}$ and $f_i = p_i f_{\parallel} + f_i^{\perp}$, we obtain

$$j_i = p_i \Gamma'' (1 - \xi) f_{\parallel} - \gamma' \lambda u_{kl} p_k p_l p_i + \Gamma' h_i^{\perp} + \Gamma'' f_i^{\perp}, \quad (\text{A4})$$

where $\xi=(\Gamma')^2/(\Gamma'')$ is a dimensionless parameter and $\gamma'=\Gamma'/\Gamma$. Similarly, the stress tensor σ_{ij}^r becomes

$$\sigma_{ij}^r = -\delta_{ij} \Pi - \frac{\lambda}{2} [p_i h_j^{\perp} + p_j h_i^{\perp}] + \frac{1}{2} [p_i h_j^{\perp} - p_j h_i^{\perp}] - \lambda p_i p_j h_{\parallel}. \quad (\text{A5})$$

The longitudinal and transverse parts of the driving force f_i are given by

$$f_{\parallel} = -\frac{C}{c_0} \mathbf{p} \cdot \nabla c - \frac{B_1 - B_3}{c_0} \mathbf{p} \cdot \nabla (\nabla \cdot \mathbf{p}),$$

$$f_i^{\perp} = \delta_{ij}^T \left[-\frac{C}{c_0^2} \partial_j c - \frac{B_1 - B_3}{c_0} \partial_j \nabla \cdot \mathbf{p} \right].$$

Similarly, the transverse part of the molecular field is given by

$$h_i^{\perp} = \delta_{ij}^T \left[\frac{B_1 - B_3}{c_0} \partial_j c + (K_1 - K_3) \partial_j \nabla \cdot \mathbf{p} + K_3 \nabla^2 p_j \right].$$

Replacing the explicit expressions of h_{\parallel} , h_i^{\perp} , f_{\parallel} , and f_i^{\perp} in Eqs. (A4) and (A5), we finally obtain

$$j_i = -\left[D(1 - \xi) p_i p_j - \frac{\gamma' w}{c_0} \delta_{ij}^T \right] \partial_j c - \gamma' \lambda u_{kl} p_k p_l p_i,$$

where $w=\Gamma(B_1-B_3)$ is a velocity and we have neglected terms of second and higher orders in the hydrodynamic fields. Finally, the reversible part of the stress tensor is given by

$$\begin{aligned} \sigma_{ij}^r = & -\delta_{ij} \Pi + \lambda p_i p_j p_k \left[\frac{B_1 - B_3}{c_0} \partial_k c + (K_1 - K_3) \partial_k \nabla \cdot \mathbf{p} + K_3 \nabla^2 p_k \right] \\ & - \frac{\lambda}{2} \left[\frac{B_1 - B_3}{c_0} (p_i \partial_j c + p_j \partial_i c) + (K_1 - K_3) (p_i \partial_j + p_j \partial_i) \nabla \cdot \mathbf{p} + K_3 (p_i \nabla^2 p_j + p_j \nabla^2 p_i) \right] \\ & + \frac{1}{2} \left[\frac{B_1 - B_3}{c_0} (p_i \partial_j c - p_j \partial_i c) + (K_1 - K_3) (p_i \partial_j - p_j \partial_i) \nabla \cdot \mathbf{p} + K_3 (p_i \nabla^2 p_j - p_j \nabla^2 p_i) \right] \\ & - \lambda \Gamma' \xi p_i p_j (D p_k \partial_k c + w p_k \partial_k \partial_l p_l) + \frac{\lambda^2}{\Gamma} p_i p_j u_{kl} p_k p_l. \end{aligned}$$

Taking $K_1=K_3=K$ leads to the equations given in Sec. I.

- [1] H. Gruler, U. Dewald, and M. Eberhardt, *Eur. Phys. J. B* **11**, 187 (1999).
- [2] J. Toner and Y. Tu, *Phys. Rev. Lett.* **75**, 4326 (1995); J. Toner, Y. Tu, and S. Ramaswamy, *Ann. Phys.* **318**, 170 (2005).
- [3] R. A. Simha and S. Ramaswamy, *Phys. Rev. Lett.* **89**, 058101 (2002).
- [4] K. Kruse, J. F. Joanny, F. Jülicher, J. Prost, and K. Sekimoto, *Phys. Rev. Lett.* **92**, 078101 (2004).
- [5] D. Saintillan and M. J. Shelley, *Phys. Rev. Lett.* **99**, 058102 (2007); **100**, 178103 (2008).
- [6] D. Marenduzzo, E. Orlandini, M. E. Cates, and J. M. Yeomans, *Phys. Rev. E* **76**, 031921 (2007).
- [7] S. Ramaswamy and M. Rao, *New J. Phys.* **9**, 423 (2007).
- [8] H. Chaté, F. Ginelli, G. Grégoire, and F. Raynaud, *Phys. Rev. E* **77**, 046113 (2008).
- [9] P. T. Underhill, J. P. Hernandez-Ortiz, and M. D. Graham, *Phys. Rev. Lett.* **100**, 248101 (2008).
- [10] A. Baskaran and M. C. Marchetti, *Phys. Rev. Lett.* **101**, 268101 (2008); *Phys. Rev. E* **77**, 011920 (2008).
- [11] T. B. Liverpool and M. C. Marchetti, *Phys. Rev. Lett.* **90**, 138102 (2003).
- [12] T. B. Liverpool and M. C. Marchetti, in *Cell Motility*, edited by P. Lenz (Springer, New York, 2007).
- [13] R. Voituriez, J. F. Joanny, and J. Prost, *Europhys. Lett.* **70**, 404 (2005).
- [14] L. Giomi, M. C. Marchetti, and T. B. Liverpool, *Phys. Rev. Lett.* **101**, 198101 (2008).
- [15] Y. Hatwalne, S. Ramaswamy, M. Rao, and R. A. Simha, *Phys. Rev. Lett.* **92**, 118101 (2004).
- [16] T. B. Liverpool and M. C. Marchetti, *Phys. Rev. Lett.* **97**, 268101 (2006).
- [17] M. E. Cates, S. M. Fielding, D. Marenduzzo, E. Orlandini, and J. M. Yeomans, *Phys. Rev. Lett.* **101**, 068102 (2008).
- [18] B. M. Haines, I. S. Aranson, L. Berlyand, and D. A. Karpeev, *Phys. Biol.* **5**, 046003 (2008).
- [19] A. Sokolov and I. S. Aranson, *Phys. Rev. Lett.* **103**, 148101 (2009).
- [20] B. M. Haines, A. Sokolov, I. S. Aranson, L. Berlyand, and D. A. Karpeev, *Phys. Rev. E* **80**, 041922 (2009).
- [21] S. A. Edwards and J. M. Yeomans, *Europhys. Lett.* **85**, 18008 (2009).
- [22] A. Baskaran and M. C. Marchetti, *Proc. Natl. Acad. Sci. U.S.A.* **106**, 15567 (2009).
- [23] The parameters β_i and α have different dimensions from those used in [12] as here we have incorporated an additional factor of ℓ^2 in their definition.
- [24] A. Maeda, M. Notomi, and K. Uchinokura, *Phys. Rev. B* **42**, 3290 (1990).
- [25] F. Jülicher and J. Prost, *Phys. Rev. Lett.* **75**, 2618 (1995).
- [26] Our sign notation for α is different from that used in [17]. In [17], the authors denoted the magnitude of the active stress by $\zeta = -\alpha$.
- [27] We neglect here convective nonlinearities in the Navier-Stokes equations that are unimportant on the long time scales of interest.